

# Non-contact non-destructive monitoring of concrete structures using pulsed Laser and microphones

Subhra Majhi<sup>1</sup>, Abhijit Mukherjee<sup>1</sup>, Nihar Sane<sup>1</sup> and Siddhant Sharma<sup>1</sup>

<sup>1</sup> School of Civil and Mechanical Engineering, Curtin University, Kent Street, Bentley, WA:6012, Australia

email: [subhra.majhi@curtin.edu.au](mailto:subhra.majhi@curtin.edu.au) (for correspondence), [abhijit.mukherjee@curtin.edu.au](mailto:abhijit.mukherjee@curtin.edu.au), [n.sane@postgrad.curtin.edu.au](mailto:n.sane@postgrad.curtin.edu.au), [s.sharma6@postgrad.curtin.edu.au](mailto:s.sharma6@postgrad.curtin.edu.au)

**ABSTRACT:** Concrete structures are at several stages of deterioration across the world. The presence of chloride ions salts as in the case of marine infrastructure or due to the application of de-icing salts, can further aggravate the rate of deterioration. Inspections of large concrete structures are predominantly undertaken through visual inspections. Detailed inspections are undertaken using piezo-generated ultrasonics. These inspections can be time and resource-intensive as the piezo devices need to contact the structure during measurements and their energy outputs are limited. Rapid inspections of large civil engineering structures would require a non-contact, high-energy source means of measurement. In our approach, we used a high-energy pulsed laser for excitation and an acoustic microphone for reception towards monitoring concrete structures. Defects in concrete like debonding and honeycombing, were simulated in the concrete specimens. The pulsed laser was used to excite the concrete specimen and the resultant waves generated due to this excitation were measured using focused cardioid microphones. The characteristic features in a typical waveform were first identified in pristine specimen. Subsequently, features corresponding to defects are extracted from the acquired signals using the signals from the pristine signal as a reference. The variations in these features were localised and their veracity was associated with the embedded defects in the specimen. As a result, the location and the nature of the defect were inferred. Thus, through this work, a framework for using pulsed lasers and microphones for non-contact non-destructive detection of defects in concrete is demonstrated.

**KEY WORDS:** Concrete structures, Pulsed laser, acoustic microphone, non-contact Condition monitoring, damage detection.

## 1 INTRODUCTION

Australia has a road network of about 14,500 km of National highways and 265,000 km of major local roads. These roads are supported by 53,000 bridges which are predominantly made of concrete [1]. According to the National State of the Asset Report in 2024, councils across Australia have concrete bridges, buildings and stormwater drains worth \$66.5bn that are in poor condition, function and capacity [2].

Traditionally, built infrastructure assets have been inspected visually, depending on the expertise of the inspectors. These assets are predominantly inspected visually which is tedious, unreliable, and expensive. Moreover, asset owners find it difficult to allocate resources for their monitoring and maintenance. So, sensors can be embedded into the assets to improve reliability in reporting their condition. Fibre optic sensors have been embedded in concrete structural assets to measure strains and sense deterioration in them [3]. As these fibres are predominantly glass fibres, they are susceptible to deterioration due to alkali attack from the concrete. Ensuring the longer durability of these sensors is a challenge [4]. Radio Frequency Identification (RFID) sensors have been embedded in concrete assets to detect changes in humidity and temperature in assets [5]. However, RFID devices are a passive means of monitoring, requiring the sensors to be embedded during the construction phase of assets.

Ultrasonic sensors generate waves that travel through the asset and interact with any emanating deterioration in it. Ultrasonic sensors can be embedded in concrete, and the condition of the concrete asset is discerned through the recorded travelling waves [6]. However, they can deteriorate over time and are prone to vandalism, making them unreliable. Moreover, these sensors must be pre-embedded in the assets before the inception of any deterioration. Mobile sensors can be used to alleviate the shortfalls in embedded sensing [7].

Image analysis and its synergistic association with computer vision have also been attempted for mobile sensing of concrete assets [8]. However, using this method, sub-surface deteriorations in the assets cannot be detected until they emerge to the surface. Mobile piezo sensors are commonly used for the generation and reception of ultrasonic waves for condition monitoring. They have been used to detect corrosion in rebars [9] and subsequently when they are embedded in concrete [10]. Field instruments that can provide scans of concrete are now available. The compact modular design of these ultrasonic scanners makes them convenient for surface-based operations [11]. The data obtained from these scanning devices can be coupled with advanced imaging algorithms to understand hidden rebars [12], incipient corrosion and debonding [13]. However, the scanning area is rather limited (around 300 mm square). Moreover, it is a manual and contact device. Thus, generating ultrasonic scans for concrete assets using mobile piezo sensors can be time and labour-intensive with contact between the sensors and the asset imperative.

In Impact Echo (IE), the surface of the concrete asset being tested is impacted with a solenoid-based metallic impactor, and the response is measured using an accelerometer. Lower frequency waves are typically used in this inspection to develop rapid scans in concrete assets [14]. These waves can also be monitored by using an array of acoustic microphones on a mobile platform [15]. The limited energy of the impactor and high attenuation of waves in concrete restrict the inspection range of this method. This impactor can be replaced with a high-energy pulsed Laser to generate high-energy pulses for rapid inspections of large concrete assets.

The range of inspections can be extended by using a high-energy pulsed laser for excitation. A pulsed laser imparts high-energy laser pulses on the substrate being monitored, making them ideal for sub-surface inspections. The energy from the

Laser pulse ablates the substrate being monitored and subsequently generates waves in the substrate [16]. These generated waves can be monitored using a range of air-coupled sensors such as acoustic microphones and Laser Vibrometers [17,18]. The laser-generated waves, when received non-contact, would help improve the inspection capabilities for large concrete assets.

In this paper, we explore the capabilities of a non-contact pulsed laser-microphone system for inspecting large concrete assets. The results and discussion of the experimental works are presented in the subsequent sections of this paper. The embedded defects in the specimens simulate some of the common defects in concrete structures.

## 2 METHODOLOGY

### 2.1 Experimental setup

In the present scheme of experiments, an Nd-YAG pulsed laser was used to excite the concrete specimen. This pulsed laser, NL303 HT, was made by Ekspla and can operate at two wavelengths 1064 and 532 nm. In the present scheme, the Laser was operated predominantly at 1064 nm with a pulse duration

causes the generation of travelling mechanical stress waves in the material. A portion of the generated stress waves leaks into the air surrounding the concrete while the other part propagates in the concrete. In the present testing regime, the pulsed Laser is operated at a lower energy such that the pulsed laser, upon impact, results in an ablative region on concrete about 1 mm in diameter. The depth of penetration of this ablative region is on a sub-millimetre scale. This laser ablation results in the generation of stress waves in concrete. Visual observations reveal that the geometry of the ablation marks on concrete was of the order of some air voids which occur in concrete while it sets. Moreover, the imparted energy of the Laser wasn't of the order to cause any severance to the structure. Moreover, this approach doesn't involve the extraction of a core from the concrete specimen. Thus, as the inspection method is relatively void of destruction to the specimen, this approach is considered a non-destructive test for assessing concrete.

The stress wave propagation in concrete interacts with any defects in concrete in its travel path. Based on the differences in acoustic impedances of the defect and the surrounding concrete, a portion of the travelling wave gets reflected towards the free surface of the concrete, causing vibrations in the air

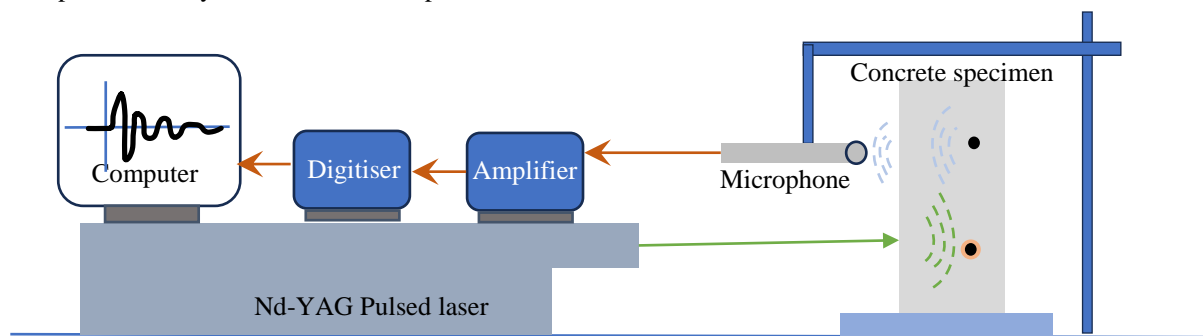


Figure 1 Experimental setup

of 3-6ns where the pulse was Gaussian in shape. The pulse repetition rate of this laser was 10 Hz. The maximum energy output from this laser was 800mJ. The waves generated from the laser impact were measured using a microphone and amplifier system. A representation of the experimental setup is shown in Figure 1. A matched pair of Røde Compact Cardioid ½'' condenser microphones was used as an air-coupled receiver. The received signals were amplified using a Yamaha MG06 mixer. The amplified signals were digitised using a Picoscope 2000 series modular oscilloscope, and subsequently, the digitised data was stored as .csv files on a personal computer. During the experiments, the specimens were securely placed on the measurement table on a positioner assisted by a guide. The Nd-YAG pulsed Laser was operated at 1064nm wavelength for excitation at an energy output of 480mJ. The microphones were placed on a rigid support and secured to the measurement table using screws as needed. An average of 32 signals is used for measurements made at any acquisition location.

As the Pulsed Laser impacts concrete, the temperature at the impact location rises to a few tens of thousands of degrees. The severe increase in temperature causes melting and ablation of material locally. As the ablation and molten material front moves ahead, it interacts with the surrounding material. This

surrounding the concrete. The vibrations in the air caused by the laser impact and subsequent reflections from embedded defects in the air surrounding the concrete are measured by acoustic microphones. The vibrations received at the microphones are digitised and amplified as required.

### 2.2 Specimen details

In this experiment, concrete specimens were cast for testing. All specimens were of the dimension 500 x 250 x 100 mm. Each specimen has two steel bars of 10 mm diameter embedded in it. The concrete specimens were prepared with a mix design by weight as shown in Table 1.

Table 1: Concrete Mix Design

Constituent	Cement	Fine aggregate	Coarse aggregate	w/c ratio
Ratio	1	1.44	2.32	0.5

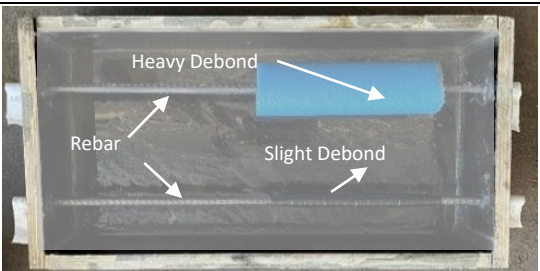
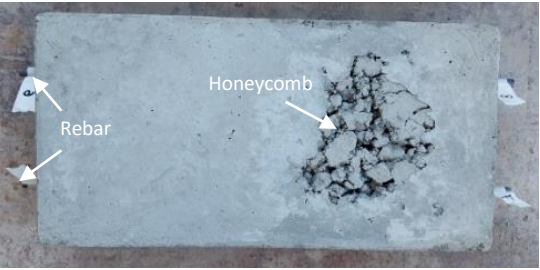
The nominal size of the coarse aggregate used was 10mm. The prepared moulds were filled in three layers, and a table vibrator was used to remove any air voids formed during casting of the specimen. After casting, the specimens were cured for 28 days in a water bath. Along with the specimen mentioned below,

cylinders of the specimen were also cast to test the cylinder compression test of the mix. The average compression strength of concrete obtained from this mix was 48.2 MPa. Table 2 demonstrates the details of the specimens used in the present study. In specimen D1, two types of debonds were created on the embedded rebars. One debond was created using a polystyrene foam wrap around the bar, representing severe debonding, and the other by wrapping several layers of insulation tape around the bar, representing slight debonding. In specimen H1, a region of honeycombing was simulated. This was created by placing aggregates of larger diameter mixed with cement without vibration in the mould and letting it set for one day before casting. Subsequently, the measurement points were marked on the specimen at distances of 50 mm. The microphones were placed 70 mm from the surface of the specimen for all measurements. As the Laser impacts on the specimen, due to ablation a travelling mechanical stress wave gets generated and is received by the microphones. The first arrival times of these waves are noted as the Time of Arrival (*ToA*). The *ToA* of the first positive peak was calculated using Equation 1.

$$ToA = \frac{d_a}{v} \quad (1)$$

Here  $d_a$  is the aerial distance between the microphone and the laser impact on the concrete specimen, and  $v$  is the velocity of sound in air. The specimens presented in Table 2 will now be tested, and the results will be reported in the subsequent sections of this paper.

Table 2 Details of specimens used in this experimental study

ID	Photograph
D1	
H1	

### 3 RESULTS AND DISCUSSIONS

#### 3.1 Specimen D1

On specimen D1, the pulsed laser was applied, and measurements were subsequently taken on three lines, namely A, B and C series. The measurement points were marked on the specimen at distances of 50 mm as shown in Figure 2. The

microphones were placed 70 mm from the surface of the specimen for all measurements. The distance between the point of laser impact and measurement using the microphone was set to 100mm. The impact and measurement locations were chosen such that they span undamaged and locations with embedded damage in the specimen. In the present study, the pulsed laser and microphone were placed on the same side of the concrete specimen while undertaking measurements. Thus, all measurements were taken in the reflection mode, where reflected waves were monitored.

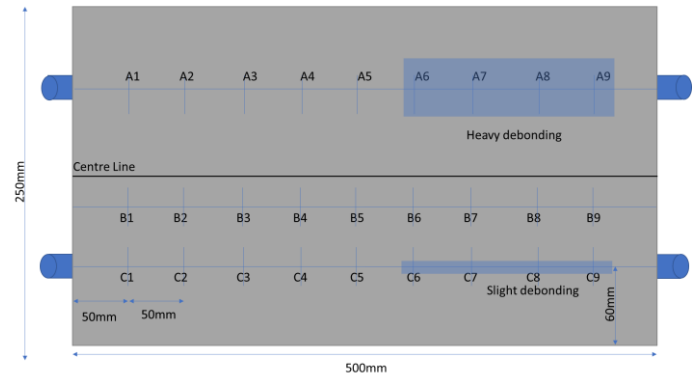


Figure 2: Specimen D1 with simulated debonding

Typical measurements from the laser-microphone acquisition setup are presented in Figure 3. This measurement is called A-Scan. Along line B, to develop an overview of the specimen condition, the laser was imparted at B8, B7, B6 etc., and the corresponding measurements were received by Microphones at positions B6, B5, B4, etc., ensuring a 100mm distance between the transmission and measurement points in the specimen. In Figure 2, the measurements' nomenclature is chosen so that it denotes the location of laser impact and microphone placement during measurements. The measurement, LaserB7\_MicB5, represents the measurement taken with a pulsed laser impacting at B7 and a microphone at B5. In Figure 3, the presented measurements denote the pristine location of the specimen. From here forth, this nomenclature will be followed for nomenclature. In these measurements presented in Figure 3, the first peak was observed between 0.3 and 0.4 ms. *ToA* of the first positive peak was calculated using Equation 1. Here, *ToA* accounts for the arrival of the Rayleigh wave to the microphone due to Laser impact on concrete.

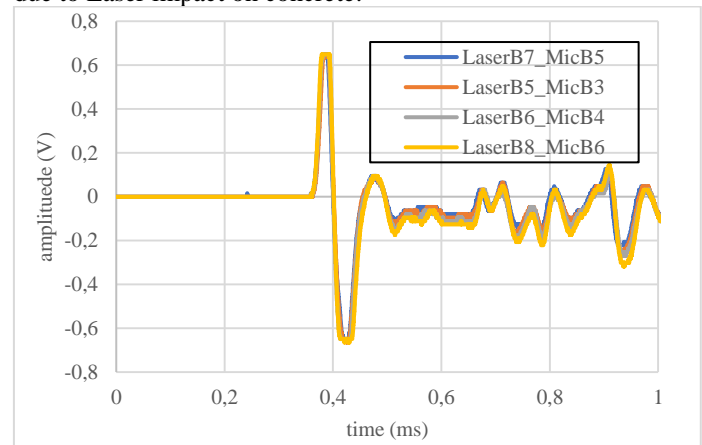


Figure 3 Repeatability of measurements

During the experiments, the Laser is aimed at a horizontal distance of 100 mm from the microphone on the concrete. The microphone is placed at a vertical distance of 70 mm from the concrete surface. For this configuration, the value of  $d_a$  was 122.06 mm. The value of  $v$  was assumed to be 343 m/s at a temperature of 25°C. Thus, the  $ToA$  was 0.35 ms as per Equation 1. As the Laser impacts the concrete surface, a stress wave is generated in the concrete due to its ablation. Upon impact, a stress wave travels in the air as well as in the concrete. The travelling stress waves in concrete have a higher velocity. The stress wave in concrete travels through the specimen and reflects from the concrete-air interface at the bottom of the specimen. The difference in acoustic impedance between concrete and air results in the generation of this reflected wave. The reflected wave now reaches the level where the laser had initially impacted. Subsequently, the reflected wave leaks into the air and reaches the microphone. The expected arrival time of this reflection is around 0.7 ms. The presence of any defects in concrete would result in a mismatch of acoustic impedances between the concrete and the defect. This acoustic impedance difference would result in the generation of a subsequent reflected wave. As the source of the reflected waves would lie before the bottom of the specimen, the reflection from embedded defects would occur before the arrival of the reflection peak. Thus, the first arrival and the arrival of the reflected peak would be considered as two markers in the measured signals. Further investigations will be undertaken to explore reflection signatures from defects in the subsequent sections.

The characteristic of this peak corresponding to the first arrival remains unchanged over the measurement undertaken on line B. Between 0.4 and 0.7 ms, several other reflections are observed. This corresponds to the arrival of the reflected waves in the specimen. Similarities in the character of the signal were observed across several measurements along line B, as presented in Figure 3. As the signals remain relatively unchanged across several locations on the specimen, the repeatability in measurements using the laser-microphone system is ascertained. Now, the variations in measurements over locations of embedded debonds will be explored to understand the capabilities of this technique for the detection of embedded damages.

Subsequently, measurements were undertaken on specimen D1 in a similar configuration. The laser-microphone measurements were taken over Lines A and C over the two rebars embedded in the specimen. Over these measurement lines, two different types of debonding were simulated. During casting, heavy debonding was simulated along line A by embedding a concentric low-density polyethylene foam of about 10 mm thickness over the rebar. Along line B, four layers of regular insulation tape were used to create the slight debonding case. The observed variation in measurements corresponding to the locations of defects is presented in Figures 4 and 5.

As observed in Figures 4 and 5, the measurements taken along lines A and C in principle have similar characteristics between 0.3 and 0.4 ms as those observed earlier over line B. This initial peak, corresponding to the arrival of Rayleigh waves, can be observed at 0.4 ms. They correspond to the measurements acquired over the simulated heavy debond and slight debond

regions are presented. In the measurements along line A, the signal amplitude varies between 0.5 and 0.7 ms in regions with the presence of an embedded heavy defect. Figure 4 shows the variation in the amplitudes in measurement LaserA6\_MicA8 in the heavy debond region over the measurement LaserA2\_MicA4. This variation is caused by the acoustic impedance introduced by the heavy *debond*.

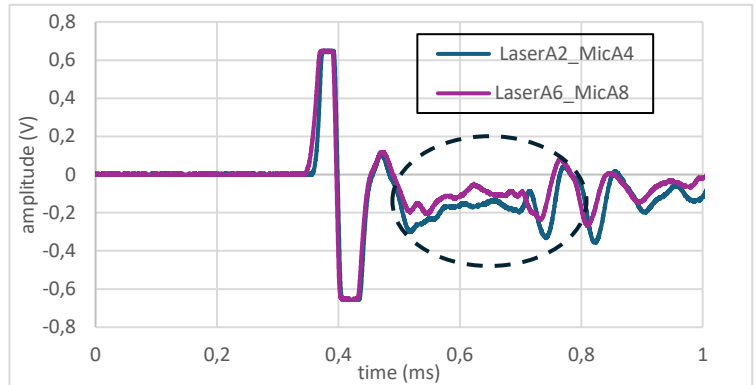


Figure 4 Measurements over simulated heavy debonding

On line C, a significantly different variation in the phase of the signal between 0.6 and 0.7 ms was observed. In the mentioned time interval, the measurement LaserC8\_MicC6, which is directly over the slight debond region, has a significantly different signature as compared to the pristine region in measurement LaserC3\_MicC1, as observed in Figure 5. This variation was on account of the change in acoustic impedance caused by the simulated slight debond that was embedded in the specimen. The variations in amplitude and phase as reflected in the signal characteristics due to the embedded effects were thus observed.

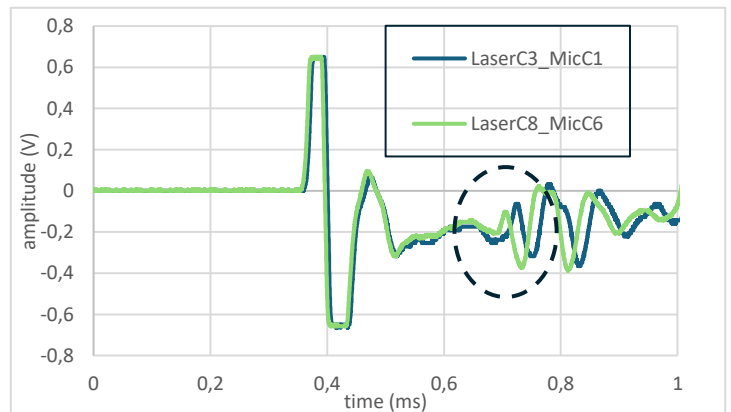


Figure 5 Measurements over simulated slight debonding

Thus, considerable changes in the waveform were observed in the specimen corresponding to the presence of embedded damages in the specimen. These changes in the waveform need to be identified and subsequently used to understand and classify the nature of damage in the specimens.

### 3.2 Specimen H1

The methodology discussed for specimen D1 will now be tried for specimen H1. Measurements are undertaken on lines A and C on this specimen as presented in Figure 6. In Figures 7 and



8, measurements taken along the lines B and C on the specimen are presented.

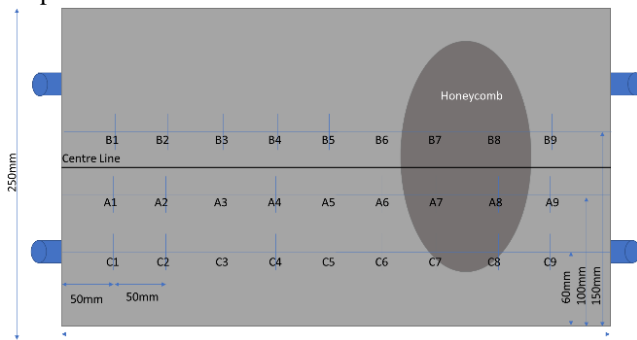


Figure 6 Specimen H1 with simulated honeycombing

The arrival time of the first peak across all measurements in this specimen is consistent with those observed in specimen D1. However, there is a considerable variation in the phase and magnitude of the signal after the first arrival between 0.4 and 0.8 ms. Along the line B, in the measurement LaserB6\_MicB8, there is a sharp rise in the amplitude and considerable variation in the phase of the signal compared to measurements at LaserB1\_MicB3. The increased difference in acoustic impedance due to air voids in the honeycomb around the LaserB6\_MicB8 points resulted in this variation in the signal. The variations in the signal between 0.4 and 0.7ms warrant further investigation to uncover details about hidden defects in the specimen (Figure 7).

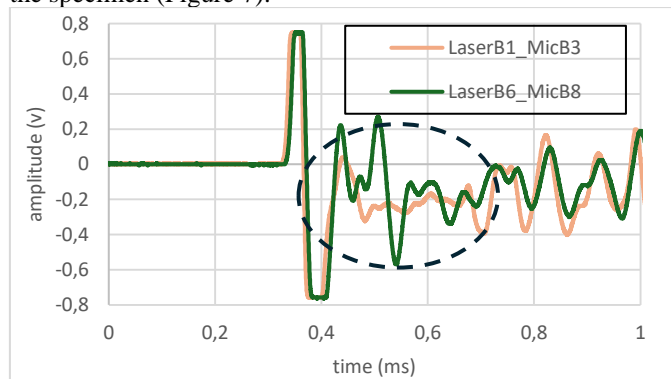


Figure 7 Signals in specimen H1 over the line B

In measurements along line C, the extent of variation in the signals is slightly lower compared to the ones over line B. In Figure 8, a variation in measurement over honeycomb, LaserC8\_MicC6, between 0.4 and 0.7ms over measurement LaserC3\_MicC1 can be observed. This trend is expected, and a plausible explanation surrounding this trend is the presence of line C further away from the core of the honeycomb. However, this variation is to be classified, and its extent is associated with the veracity of the damage in the specimen.

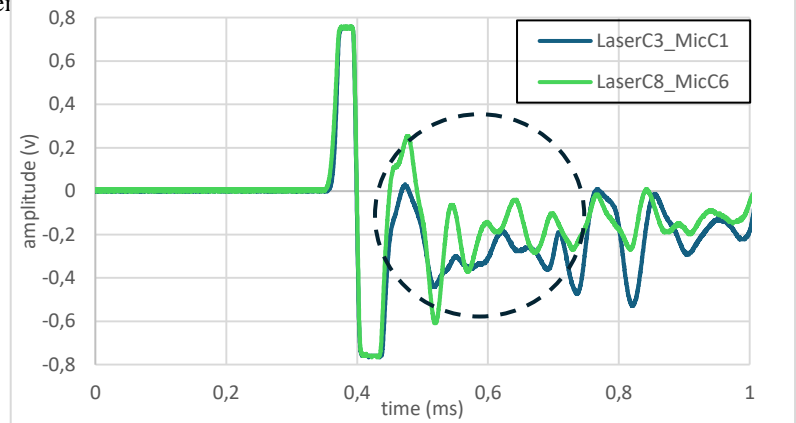


Figure 8 Signals in specimen H1 over the line C

### 3.3 Classification of defects

To further understand and classify the variations in the acquired signals due to embedded damages. The acquired signals are compared with the measurements at the pristine region. A Condition Index ( $CI$ ) is proposed to compare the signals acquired at various locations in the specimens. Though there are several approaches to compare two vectors, the proposed approaches are used for its simplicity and ease of computation. To undertake this comparison, the signals in the comparison are considered vectors. The vectors are unitised by dividing them by their magnitude. The process of unitising a vector is presented in Equation 2 by considering the example of a pristine signal. Here  $V_p$  is the signal and  $V_{pu}$  is its corresponding unitised vector.

$$V_{pu} = \frac{V_p}{\|V_p\|} \quad (2)$$

Subsequently, unitised vectors of measurements from other damage locations are also developed. Using scalar products, the similarities of the developed vectors are evaluated. The scalar product of these vectors is presented in Equation 3. The scalar product is captured in a parameter  $CI$ .

$$CI = V_{pu} \cdot V_{du} \quad (3)$$

Here  $V_{du}$  represents the unitised vector from an A-Scan acquired over a defect. This is compared with the  $V_{pu}$  calculated over the pristine region.

The outcome of Equation 3 is  $\cos \theta$ , where  $\theta$  represents the angle of the two unitised vectors. If  $CI = 1$ , the corresponding  $\theta$  between the vectors is 0, which implies the vectors are identical to each other. As the value of  $\theta$  increases, the value of  $CI$  decreases. Thus, the value of  $CI$  indicates the difference between the signal at a location with the pristine signals. Now,  $CI$  at several locations will be compared with the pristine signal to understand its association with the location of damage in the specimens.

To undertake the comparison, an average of three measurements recorded at LaserB5\_MicB3 on specimen D1 over line B was utilised and as  $V_{pu}$  as per Equation 2. Subsequently, three other pristine locations on this specimen were considered as  $V_{du}$  and their  $CI$ s calculated as per Equation 3. In Table 3, a comparison of  $CI$  values at various locations in the pristine region is presented. These values are very close to each other, indicating that the time signals are like each other.

Table 3 CI over the line C for pristine condition

Location	CI
Pristine1	0.993458
Pristine2	0.986087
Pristine3	0.990595

As the reliability of measurements was observed earlier over the pristine location, an average of the three measurements recorded at the pristine region will now be used as a reference pristine signal. The variation in *CI* at the damage will now be explored to understand the sensitivity of the proposed approach in detecting damage. This will be compared against the measurements taken over the defect regions. As seen in Table 4, a low *CI* value was observed at the debond region. This variation occurred because of the variation in the acquired signal due to the acoustic impedance difference between the surrounding concrete and the simulated debond in specimen D1. This variation in acoustic impedance causes the incident wave to reflect, thus the variation in the wave signature. The magnitude of *CI* further reduces over the honeycomb region in specimen H1. The air present in the simulated honeycomb results in further variation in acoustic impedance and thus a further decrease in *CI* value.

Table 4 Variation in signal similarities at various locations

Location	CI
Heavy debond	-0.08175
Slight debond	-0.08782
Honeycomb1	0.050011
Honeycomb2	0.001647

The veracity of the proposed methodology in detecting hidden damages in concrete is thus established. Further investigations are now underway to explore the capabilities of the proposed method to evaluate the veracity of this method in deciphering defects at various depths from the surface. This will be extended to detecting progressive deterioration. Monitoring long-term durability due to the actions of corrosion and freezing-thawing will be explored.

#### 4 FREQUENCY RESPONSE

To understand the variation in A-Scans due to defects, the acquired time signals will now be explored to understand the frequency content in them. The frequency content in the signal was developed through the Fast Fourier Transform algorithm implemented using the ‘fft’ function in MATLAB software [19]. The frequency content of signals is presented in Figure 9. A high-pass filter with a cut-off set at 2 kHz was used on the frequency response to remove any ambient vibrations in the signal. The frequency response of the pristine sample was compared with that of the defect cases discussed earlier. It can

be observed that the signal has considerable signal strength between 6 and 15 kHz across all measured signals. The magnitude of the frequency spectra across all the damage cases is higher than the pristine case. Moreover, there is an increase in the magnitudes of lower frequency components, particularly between 6 and 12 kHz and a damping down of frequencies higher than that range. This indicates a change in the vibration characteristic of the specimen. To explore the trends in the frequency responses, regions of interest will be identified, and the frequency content in the regions will be explored. Further information can be inferred from the inclusion of information about the phase spectra of the acquired signal.

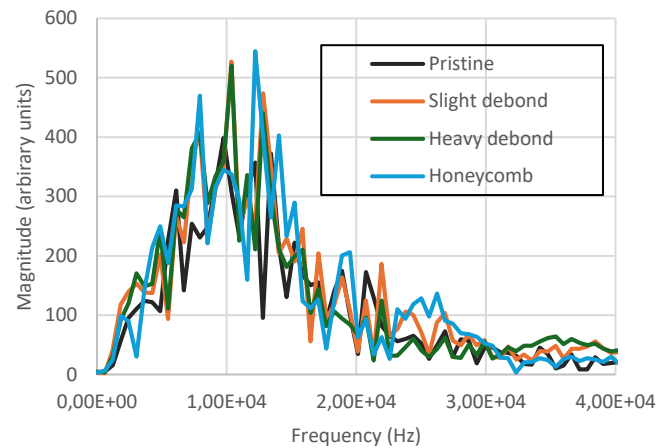


Figure 9 Frequency responses of A-Scan signals

#### 5 CONCLUSIONS

In this paper, we present a novel pulsed-laser microphone system to monitor deterioration in concrete. In this method, high-energy pulses are used to generate acoustic waves and microphones are used for reception. The efficacy of this non-contact, non-destructive method for monitoring hidden deterioration in concrete is explored in this study. The following are the key conclusions:

- In this study, the generation of acoustic elastic waves in concrete using a Pulsed Laser and their reception using an acoustic microphone was established.
- The variation in acoustic wave pressure due to laser impact was received by the microphone and digitised into an electrical signal.
- The signals were acquired on two specimens with embedded defects like simulated debonding and honeycombing.
- The variation of signals in the pristine region and the defects was identified.
- A Condition Index (*CI*) was developed to qualify the variation of signals due to the presence of defects.
- The efficacy of using a pulsed laser–acoustic microphone system in detecting embedded defects was established.

## ACKNOWLEDGMENTS

The authors would like to acknowledge the support from SmartCrete CRC on project number 21.PP.0112 titled 'Digital twin of reinforced concrete infrastructure for intelligent asset management'. The support from Curtin University technical staff in fabricating the moulds for the concrete specimens used in this work is kindly acknowledged.

## REFERENCES

- [1] C. Caprani. (2018, August 22, 2018) Are Australian bridges safe, and can we do better? *The Conversation*. Available: <https://theconversation.com/are-australian-bridges-safe-and-can-we-do-better-101825>
- [2] Australian Local Government Association. (2024). *2024 National State of the Assets Report*. [Online] Available: <https://alga.com.au/app/uploads/ALGA-2024-National-State-of-the-Assets-Technical-Report.pdf>
- [3] S. Villalba and J. R. Casas, "Application of optical fiber distributed sensing to health monitoring of concrete structures," *Mechanical Systems and Signal Processing*, vol. 39, no. 1-2, pp. 441-451, 2013.
- [4] H. Qiao, Z. Lin, X. Sun, W. Li, Y. Zhao, and C. Guo, "Fiber optic-based durability monitoring in smart concrete: A state-of-art review," *Sensors*, vol. 23, no. 18, p. 7810, 2023.
- [5] P. Pursula, I. Marttila, K. Nummila, and H. Seppä, "High frequency and ultrahigh frequency radio frequency identification passive sensor transponders for humidity and temperature measurement within building structures," *IEEE Transactions on Instrumentation and Measurement*, vol. 62, no. 9, pp. 2559-2566, 2013.
- [6] X. Wang, J. Chakraborty, A. Bassil, and E. Niederleithinger, "Detection of Multiple Cracks in Four-Point Bending Tests Using the Coda Wave Interferometry Method," *Sensors*, vol. 20, no. 7, p. 1986, 2020.
- [7] J. F. Scherr and C. U. Grosse, "Delamination detection on a concrete bridge deck using impact echo scanning," *Structural Concrete*, vol. 22, no. 2, pp. 806-812, 2021.
- [8] C. Koch, K. Georgieva, V. Kasireddy, B. Akinci, and P. Fieguth, "A review on computer vision based defect detection and condition assessment of concrete and asphalt civil infrastructure," *Advanced engineering informatics*, vol. 29, no. 2, pp. 196-210, 2015.
- [9] S. Majhi, A. Mukherjee, N. V. George, and B. Uy, "Corrosion detection in steel bar: A time-frequency approach," *NDT & E International*, vol. 107, p. 102150, 2019.
- [10] S. Majhi, L. K. Asilo, A. Mukherjee, N. V. George, and B. Uy, "Multimodal monitoring of corrosion in reinforced concrete for effective lifecycle management of built facilities," *Sustainability*, vol. 14, no. 15, p. 9696, 2022.
- [11] K. Hoegh, L. Khazanovich, and H. T. Yu, "Ultrasonic tomography for evaluation of concrete pavements," *Transportation Research Record*, vol. 2232, no. 1, pp. 85-94, 2011.
- [12] S. Majhi, A. Mukherjee, and A. Ganguli, "Enhanced ultrasonic imaging in concrete structures with spatial apodization filters," *Journal of Materials in Civil Engineering*, vol. 33, no. 10, p. 04021266, 2021.
- [13] Y. Wang, A. Mukherjee, and A. Castel, "Non-destructive monitoring of incipient corrosion in reinforced concrete with top-bar defect using a combination of electrochemical and ultrasonic techniques," *Construction and Building Materials*, vol. 360, p. 129346, 2022.
- [14] H. Azari, S. Nazarian, and D. Yuan, "Assessing sensitivity of impact echo and ultrasonic surface waves methods for nondestructive evaluation of concrete structures," *Construction and Building Materials*, vol. 71, pp. 384-391, 2014.
- [15] R. Groschup and C. U. Grosse, "MEMS microphone array sensor for air-coupled impact-echo," *Sensors*, vol. 15, no. 7, pp. 14932-14945, 2015.
- [16] S. Majhi, A. Mukherjee, N. V. George, V. Karaganov, and B. Uy, "Corrosion monitoring in steel bars using Laser ultrasonic guided waves and advanced signal processing," *Mechanical Systems and Signal Processing*, vol. 149, p. 107176, 2021.
- [17] J. F. Scherr, J. Kollofrath, J. S. Popovics, B. Bühling, and C. U. Grosse, "Detection of Delaminations in Concrete Plates Using a Laser Ablation Impact Echo Technique," *Journal of Nondestructive Evaluation*, vol. 42, no. 1, p. 11, 2023.
- [18] V. Vierhub-Lorenz, C. S. Werner, K. Weiher, C. Heinze, and A. Reiterer, "Laser-based measurement system for the detection of delamination in tunnel linings," in *Optical Measurement Systems for Industrial Inspection XIII*, 2023, vol. 12618: SPIE, pp. 526-531.
- [19] The MathWorks, Inc., MATLAB version: 9.7.0.1190202 (R2019b).